Report on Development of Critical Field Testing and Site Characterization Techniques

Fuel Cycle Research & Development

Prepared for

U.S. Department of Energy
Used Fuel Disposition

Jim Houseworth

Lawrence Berkeley National Laboratory

September, 2012

FCRD-UFD-2012-000251

FCT Quality Assurance Program Document Revision 1 08/19/2011

Appendix E
FCT Document Cover Sheet

Name/Title of Deliverable/Milestone	Report on Development of Critical Field Testing and Site Characterization Techniques
Work Package Title and Number	Natural Systems Evaluations – LBNL FT-12LB080706
Work Package WBS Number	1.02.08.07
Responsible Work Package Manager	Hui-Hai Liu (Name/Signature)
Date Submitted	8-28-2012

Quality Rigor Level for Deliverable/Milestone ☐ QRL-3 ☐ QRL-2 ☐ QRL-1 ☒ N/A ☐ Nuclear Data

This deliverable was prepared in accordance with Lawrence Berkeley National Laboratory
(Participant/National Laboratory Name)

QA program which meets the requirements of
☒ DOE Order 414.1 ☐ NQA-1-2000 ☐ Other

This Deliverable was subjected to:

☐ Technical Review ☐ Peer Review

Technical Review (TR)

Review Documentation Provided

☐ Signed TR Report or,
☐ Signed TR Concurrence Sheet or,
☐ Signature of TR Reviewer(s) below

Peer Review (PR)

Review Documentation Provided

☐ Signed PR Report or,
☐ Signed PR Concurrence Sheet or,
☐ Signature of PR Reviewer(s) below

Name and Signature of Reviewers

_____ _____

_____ _____

_____ _____

***NOTE** *In some cases there may be a milestone where an item is being fabricated, maintenance is being performed on a facility, or a document is being issued through a formal document control process where it specifically calls out a formal review of the document. In these cases, documentation (e.g., inspection report, maintenance request, work planning package documentation or the documented review of the issued document through the document control process) of the completion of the activity along with the Document Cover Sheet is sufficient to demonstrate achieving the milestone. QRL for such milestones may be also be marked N/A in the work package provided the work package clearly specifies the requirement to use the Document Cover Sheet and provide supporting documentation.*

This page is intentionally blank.

CONTENTS

FIGURES

TABLES

ACRONYMS

BRI	brittleness index
OCR	overconsolidation ratio
SGR	shale-gouge ratio
UCS	unconfined compressive strength
USGS	United States Geological Survey

1. INTRODUCTION

Argillaceous rock is one rock type being considered for geologic disposal of high-level radioactive waste. A key characteristic for waste isolation is very low permeability (from 10^{-17} m^2 to 10^{-23} m^2, Neuzil, 1994) that is typically considered a barrier for groundwater flow. The low permeability characteristic is also enhanced by the mechanics of argillaceous rock; brittle fracturing in an argillaceous rock is typically followed by fracture self-sealing once the conditions leading to rock failure have abated. The ability of an argillaceous rock to provide a low permeability environment over long time periods is affected by conditions of rock stress and stress history, diagenetic alteration, and pore fluid pressure (Nygård et al., 2006). As it turns out, pore pressure is a critical component related to brittle fracturing in argillaceous rock.

Low-permeability environments are also known for their potential to develop abnormal pressure (Horseman et al., 1996). Abnormal pressure is often defined as a deviation from hydrostatic pressure, although Horseman et al. (1996) suggest that a more appropriate definition is any pressure that is inconsistent with classical, steady-state, single-phase groundwater flow. This definition eliminates common topographic effects on groundwater pressure as a cause of abnormal pressure. Although abnormal pressure is more commonly found at depths greater than 1000 m (Swarbrick and Osborne, 1998), shallower occurrences at depths of 600 m or less have been observed (Chapman, 1972, Dugan et al., 2003). Abnormal pressure is observed in many different geologic environments and is caused by a wide variety of mechanisms. Abnormal pressure is relatively common for low-permeability rock, although direct measurements of pressure conditions in low-permeability rock remain problematic. Pressure conditions are typically inferred from measurements in adjacent, more permeable formations, or are inferred from indirect measurements that require significant interpretation.

Observations of argillaceous rocks indicate that natural fracturing processes have occurred and that fracturing is likely to be related to the occurrence of abnormal pressure (Cosgrove, 2001). Fracturing in combination with abnormal pressure is associated with pressure relief and dewatering of sediments. Therefore, fractures also serve as fluid discharge pathways through low-permeability rock. Once pressure conditions that led to fracturing have abated, fractures tend to close and self-sealing occurs in which permeability of the fractures returns to a levels corresponding to a non-fractured condition. Self-healing is also possible, although some evidence of fractures that have closed but not healed exist (Arnould, 2006). Fractures that have self-sealed may be difficult to identify by visual inspection. Self-sealing of fractures is disrupted if flow through the fracture results in deposition of other materials, such as mobilized sand.

Induced hydraulic fracturing has recently become an important technique for extracting petroleum resources from argillaceous rock (Warpinski et al., 2012). Hydraulic fracturing has been used for several decades for petroleum extraction. In the past, the main application was to stimulate declining well production caused by formation damage occurring locally around wells (Parker et al., 1994). However, it has also been long used to stimulate production from low-permeability gas reservoirs (Holditch, 1979). Although there are some common technical issues linking induced hydraulic fracturing for petroleum production and natural fracturing processes of interest for radioactive waste disposal, recent developments for this specific technology are not the focus of this report.

A review of processes and conditions that lead to overpressure and measurement methods to detect overpressure are presented. The potential for fracturing to occur as a result of abnormal pressure is discussed in terms of simple fracture criteria. A model is developed and used to examine the fluid flow behavior of transient depressurization within an overpressured aquifer and low-permeability argillaceous rock. The model is also used to investigate the potential transport and disposition of natural tracers within the overpressure aquifer and within the seal penetrated by the hydrofracture during the depressurization flow process. Finally, transport of a solute (such as a radionuclide) is considered as a result of strong fluid depressurization flow through a hydrofractured seal.

2. ARGILLACEOUS ROCK

There is not a single agreed-upon definition for argillaceous rock and the term is not used consistently in the literature. Here, argillaceous rock is defined as a general category encompassing fine-grained sedimentary rock that is either predominately clay-sized particles or clay and silt. Clays are the finest-grained classification of sedimentary material so there is no lower limit for clay grain size; the specific upper limit varies by discipline, but ranges from 1 to 4 μm (Guggenheim and Martin, 1995). Silt is coarser than clay, having grain sizes between 4 μm to 63 μm.

Although grain size is extremely important characteristic for the hydrologic characteristics of clay rock, mechanical characteristics rely on mineral composition. According to the definition set out by Guggenheim and Martin (1995), clay materials have the characteristics of showing plastic behavior at sufficiently high water content and harden upon drying. Clays are distinct from clay minerals which are more specifically phyllosilicate minerals. Bain (1971) presents the plasticity of different phyllosilicate clay materials. Plasticity is defined as the difference between the Atterberg liquid limit and plastic limit. The liquid limit is the percentage by weight of water relative to the oven-dried clay where the clay-water mixture flows as a liquid. The plastic limit is the percentage by weight of water relative to the oven-dried clay where the clay-water mixture is malleable (White, 1949). Kaolinite has relatively low plasticity and sodium montmorillonite has high plasticity, with calcium montmorillonite and illite lying at intermediate levels of the plasticity index. Clay plasticity is an important aspect of argillaceous rocks in terms of their ability to express mechanical failure as a ductile shear process under some conditions while under other conditions failure results in brittle fracturing. These differences are significant for the hydrogeological behavior of clay rock. Clay plasticity also plays an important role in other hydro-mechanical behavior such as self-sealing processes for fractures in argillaceous rock.

Definitions related to argillaceous rock and rocks containing significant quantities of clay are given in Table 1. Argillaceous rock is formed initially from unlithified clay and silt, (Potter et al., 2005). Clays have more than 2/3 clay-sized particles, silts have more than 2/3 silt-sized particles, and an intermediate mixture of clay and silt is called mud. Lithification of clay, mud, and silt produces claystone, mudstone, and siltstone if the lithification does not result in laminations; otherwise lithification results in shale, which may be subdivided into clay-shale, mud-shale, and silt-shale based on the underlying source material. The USGS identifies mudstone as a general term that includes claystone, siltstone, shale and argillite. The USGS restricts the term shale to mean a lithified claystone that contains laminations (USGS) and defines argillite as a claystone, shale or siltstone that has been further lithified but lacks clear lamination. Lithification involves the processes of burial compaction and chemical diagenesis. Compaction, chemical diagenesis and

lithification affect the rock strength or stiffness; a lower-strength rock associated with a lower degree of lithification is described as "plastic" whereas a higher-strength rock associated with a higher degree of lithification is described as "indurated". Although not included in the classification shown in Table 1, another important aspect of argillaceous rock mineralogy is organic content, which can impact the formation and diagenesis of argillaceous rock (Aplin and Macquaker, 2011).

Table 1. Argillaceous rock definitions (Potter et al., 2005; USGS)

Term	**Definition**
Mudstone	A general term that includes claystone, siltstone, shale, and argillite, and that should be used only when the amounts of clay-sized and silt-sized particles are not known or specified, or cannot be precisely identified.
Claystone	indurated rock having more than 67% clay-sized minerals.
Shale	A laminated, indurated rock having more than 67% clay-sized minerals.
Argillite	A compact rock derived either from mudstone or shale, that has undergone a somewhat higher degree of induration than mudstone or shale but is less clearly laminated than shale and without its fissility, and that lacks the cleavage distinctive of slate.
Siltstone	An indurated silt having the texture and composition of shale but lacking its fine lamination or fissility; a massive mudstone having more than 67% silt-sized particles.

3. ARGILLACEOUS ROCK AND ABNORMAL PRESSURE

Abnormal pressure in the subsurface refers to fluid pressure that differs from hydrostatic pressure and is often associated with low permeability formations. There are several reasons why abnormal pressure is associated with low-permeability argillaceous formations. The low permeability of argillaceous rocks can require long periods of time to dissipate pressure deviations from hydrostatic pressure. In this context, abnormal pressure represents a disequilibrium condition that is in the process of moving towards equilibrium. However there are also natural steady-state flow and even static fluid conditions that can cause abnormal pressure.

Geologic forcing mechanisms that can cause abnormal pressure have been identified and summarized by several researchers (Neuzil, 1995; Swarbrick and Osborne, 1998; Martinsen, 1994). These mechanisms represent a wide variety of processes such that the potential for generating abnormal pressure exists in a wide range of geologic environments. Osborne and Swarbrick (1997) identified the geologic forcing mechanisms as belonging to three classes: mechanical processes affecting rock stress (e.g., burial compaction and tectonic stress); processes that affect mineral and fluid properties resulting in volume change (e.g. thermal expansion and water evolution from mineral alteration); and static and dynamic fluid mechanical processes (e.g., topographic flow and fluid buoyancy).

3.1 Abnormal Pressure from Mechanical Processes

The formation of an argillaceous rock starts with deposition of primary fine-grained clay and mud sedimentary materials. The process of burial leads to increased overburden stress over time and this stress causes compaction of the materials' porosity. Because the porosity is filled with water, which has a relatively small value of compressibility, the compaction of porosity requires expulsion of pore water. In cases such as argillaceous rock, the low permeability may cause a significant resistance to fluid flow to expel the pore water; instead fluid pressure builds up creating an abnormal pressure condition. Therefore, there is a direct link between overpressure caused by burial compaction and the evolution of the porosity of the rock; overpressured systems show higher porosity than systems that maintain pressure equilibrium in a normal compaction process. As noted by Osborne and Swarbrick (1997), this process is dynamic and rates of burial must be high enough to exceed the capacity of the compacting argillaceous rock to expel pore fluid. Conditions that favor this mechanism are a thick deposit of low permeability material and rapid burial.

In addition to gravitational loading that occurs during burial compaction, rock stress is also affected by tectonic displacements. These stresses often are imposed as horizontal compression or extension forces on the rock rather than vertical as for burial compaction, but influence pore pressure similarly (Managa and Wang, 2007). Tectonic pressures can occur rapidly as a result of fault slippage through direct changes in mechanical stress and as a result of transmission of fluid pressure through faults that have been reactivated by slippage (Sibson, 1990). Changes in tectonic stress as a result of individual fault displacements are on the order of 1 MPa (Gonçalvès et al., 2004). While 1 MPa appears to be a typical stress drop caused by an earthquake, Gough and Gough (1987) report that stress drops during earthquakes can range up to 60 MPa. Stress drops caused by earthquakes also show a trend of increasing stress drop with the depth of the earthquake (Hartzell and Brune, 1977). Richardson and Solomon (1977) reported on observations of intraplate earthquakes and found that stress drops ranged from 0.1 to 7 MPa.

3.2 Abnormal Pressure from Changes in Fluid or Rock Volume

Processes that cause a change in rock or fluid volume are another class responsible for the generation of abnormal pressure. Such volume changes can occur as a result of heating (called aquathermal heating) during burial or by the introduction of external sources from hydrothermal activity. Heating causes thermal expansion of argillaceous rock and water, with water expanding more than rock (Martinsen, 1994). If the expanded volume of water cannot be discharged fast enough, there will be an increase in fluid pressure. A very broad class of processes that are typically considered a part of diagenesis or metamorphism include mineral alteration that results in the evolution of water or precipitation of minerals, or both. Examples include smectite dehydration and smectite to illite and gypsum to anhydrite mineral transformations. Smectite dehydration, in which water is released from clay interlayers, is sensitive to fluid pressure and temperature. An increase in fluid pressure leads to an increase in the dehydration temperature. If dehydration results in a pressure increase, it will inhibit further dehydration. Therefore, smectite dehydration is not considered a likely mechanism for creating abnormal pressure (Colten-Bradley, 1987). Smectite transforms to illite at temperatures in excess of 60 °C and releases water bound in the smectite clay interlayers. In addition to the release of water, the smectite to illite transformation releases Si, Ca,

Fe, and Mg ions. This can lead to precipitation of minerals and a reduction in both porosity and permeability caused by the precipitate (Osborne and Swarbrick, 1997).

Another consideration is that mineral transformations may also affect the mineral framework of the argillaceous rock. The transformation of smectite to illite is usually accompanied by dissolution of potassium feldspar or mica (Altaner, 1986; Boles and Franks, 1979). The mineral transformation from smectite to illite requires potassium, available from the potassium feldspar or mica. Sodium released from the smectite typically transforms any calcium-bearing feldspars to albite. Feldspar grains are generally larger than the smectite clays and play a significant role in the load-bearing mineral structure. These and other mineral reactions associated with smectite to illite reactions result in changes in the load-bearing secondary grains commonly present in smectite. These changes cause mineral compaction and load transfer from the mineral to the pore water, causing an increase in pore pressure (Lahann and Swarbrick, 2011).

Gypsum transforms to anhydrite at 40-60 °C and in the process releases 2 moles of water per mole of gypsum resulting in a loss of 39% bound water by volume and a similar volume decrease of 38.5% (Swarbrick and Osborne, 1998; Osborne and Swarbrick, 1997; Zanbak and Arthur, 1984). This volume decrease will also result in load transfer mechanisms driving up pore pressure.

3.3 Abnormal Pressure from Static and Dynamic Fluid Mechanical Processes

The final class of abnormal-pressure generating mechanisms is associated with fluid statics and fluid-flow dynamics. One example is the change in pressure gradient when moving vertically from a reservoir brine section up through a hydrocarbon resource. This shows how abnormal pressures are generated through fluid statics involving fluids with different densities. An example of abnormal pressure caused by flow dynamics occurs in the Pierre shale in Colorado (Belitz and Bredehoeft, 1986). Recharge moves downward through the low-permeability Pierre shale into a higher-permeability Dakota sandstone formation that directs the flow subhorizontally to a discharge point at the ground surface. Because of the high flow resistance within the shale, a large portion of the piezometric head is dissipated within the shale and results in abnormally low pressure within the lower part of the shale and in the Dakota sandstone. Such topographic flow phenomena can also lead to abnormal overpressure (Wolf et al., 2009). Certain mechanisms, such as osmotic flow and buoyancy can lead to static or quasi-static conditions in the presence of abnormal pressure. For example, abnormal pressure is associated with salinity gradients in shales because of the ability of these rocks to act as semi-permeable membranes (Neuzil and Provost, 2009). If the shale, containing a higher-salinity pore water, is exposed to a lower salinity water on its boundary, osmotic forces will result in water being imbibed into the shale. This will lead to a counter-balancing pressure gradient that can attain a static equilibrium with the osmotically-driven flow process. Neuzil (2000) found that osmotic pressure effects were more likely to occur in lower porosity sedimentary systems (less than 0.05) that usually are found at depths over 5 km, or in shallower systems that had been buried to such depths prior to uplift. Static equilibrium in the presence of abnormal pressure is a typical condition for hydrocarbon traps in which the lower-density hydrocarbon fluid is trapped against a shale caprock. The water-saturated caprock presents a capillary barrier to further movement of the hydrocarbon into the caprock. The trapped, static, hydrocarbon results in an abnormal static pressure within the reservoir. Another process that is transitional between rock mechanical and fluid mechanical are stresses transmitted as a result of

salt or mud diapirism, a process by which more ductile salt or argillaceous rock is forced up through more brittle rocks via the buoyant forces acting on the salt or argillaceous rock relative to the surrounding rock, rock stress, and fluid pressure at the source.

3.4 Equilibration Time for Abnormal Pressure

Fluid pressure in argillaceous rock can retain pressure disequilibrium for long time periods in close proximity with lower-pressure conditions in surrounding formations because of the very low permeability typical of argillaceous rock. Typically, the pressure sink for a low-permeability argillaceous rock is an adjacent higher-permeability aquifer. Thus, pressure is transmitted and dissipated across the argillaceous layer thickness. A standard approximation describing transient flow in a saturated rock is that pressure is transmitted as a diffusive process in which the pressure diffusion coefficient, also known as the hydraulic diffusivity, is the rock's hydraulic conductivity divided by the volumetric specific storage coefficient. The time scale for pressure dissipation is $h^2/4D_h$, where h is the layer thickness, and D_h is the hydraulic diffusivity. For example, an argillaceous rock with a hydraulic conductivity (K_h) of 10^{-13} m/s (equivalent to a permeability of about 10^{-20} m^2) and a specific storage coefficient (S_s) of 10^{-5} m^{-1}, has a hydraulic diffusivity, $D_h = K_h/S_s$, of 10^{-8} m^2/s. The time scale for pressure dissipation in a 100-m thick argillaceous formation is on the order 10,000 years. Given an order of magnitude uncertainty in hydraulic diffusivity (Gonçalvès et al., 2004), the equilibration time can vary between 1,000 and 100,000 years. Although aquifer hydraulic diffusivities are much higher, the ultimate equilibration of excess pressure in an aquifer may require long-distance transmission of pressure along the aquifer to a pressure sink, such as an outcrop. Therefore, the time for dissipation of a pressure anomaly in an aquifer may be as long as for pressure dissipation in low-permeability rock (Gonçalvès et al., 2004).

4. IN-SITU MEASUREMENT METHODS FOR PRESSURE IN ARGILLACEOUS ROCK

As stated earlier, the development of abnormal pressure requires the presence of a low-permeability formation. Formation pressures in permeable zones are measured during well drilling using drill-stem tests or wireline pressure testing (Bredehoeft, 1965; Brown, 2003). Both tests require fluid to flow from the formation. For a drill-stem test this involves fluid flowing into a packed-off section of the wellbore and for a wireline pressure test, the fluid flows into a chamber that is sealed against the formation. While these methods are suitable for more permeable formations, the time for pressure equilibration with the wellbore drill stem tests or formation testing apparatus is too long for practical use of such methods. A general issue concerning pressure measurements is that drilling can supercharge the formation pressure because drilling fluids are typically weighted to operate at pressures above the expected formation pressure. Although one of the functions of drilling muds is to help prevent fluids from entering the formation, some formation leakage is expected, along with changes in formation pressure locally around the borehole.

Because direct methods to measure fluid pressure in low-permeability formations are impractical, alternative methods for estimating in-situ pressure of these formations have been developed. The

most widely used method is based on the Terzaghi concept of effective stress (Swarbrick 2002, Stump et al., 1999). Effective stress is equal to the total stress minus the pore pressure. Total stress can be calculated from the vertical and horizontal stress components. Vertical stress is more easily estimated from the weight of the overburden rock and fluids. Because horizontal stresses can be difficult to estimate, the vertical overburden stress is sometimes used to represent total stress (Fertl and Chilingarian, 1987). The greatest challenge is to estimate the effective stress. This is done through an association between the porosity of the system and depth for normally-compacted sediment. As sediments compact and dewater with increased burial, the porosity decreases. Cases in which the sediment is able to release water during burial compaction such that the fluid pressure remains hydrostatic are considered normally compacted. Normal compaction results in a unique relationship between porosity, depth, and effective stress. Various geophysical measurements for estimating porosity can be used to identify the effective stress through its relationship with porosity given a normal compaction curve (Swarbrick, 2002). The difference between the total stress and effective stress give the formation pore pressure.

Swarbrick (2002) summarizes a number of pitfalls related to indirect pressure estimation based on effective stress. There are several reasons that the indirect pressure method may fail related to defining the normal compaction curve, quantifying total stress, and processes affecting compaction other than burial overburden stress. These include (1) initiation of overpressure at shallow depths, restricting the availability of information on normal compaction; (2) lithological variability causing discrepancies with the normal compaction curve; (3) inability to estimate and incorporate horizontal stresses in the total stress; (4) overpressure caused by fluid expansion, such as smectite to illite dewatering, which can affect the strength of the mineral skeleton causing a departure from normal compaction relationships between effective stress and porosity; and (5) non-mechanical compaction, such as deposition of secondary minerals, that also causes a departure from normal compaction relationships between effective stress and porosity. Swarbrick (2002) concludes that these factors typically result in an underestimate of pore pressures when using an indirect pressure method.

Alternative methods for determining pressure in clay formations directly have been used for geotechnical applications at an offshore petroleum operation on the Norwegian continental shelf (Strout and Tjelta, 2005). Two pressure measurement methods were implemented, dissipation tests and piezometers. Dissipation tests are conducted by inserting a narrow-diameter probe into the clay and measuring the pressure response. Pressure initially rises caused by compression of the soil displaced by the probe. Dissipation of the excess pressure to an equilibrium level provides a measure of the pore pressure in the clay. Equilibration time is a function of the probe dimensions and formation permeability. As for direct methods, these times can restrict the practicality of the method. Direct placement of piezometers in the formation has also been used and generally produced more reliable results. Although this method requires similar or longer times for equilibration, after installation the piezometer can operate and record data autonomously. The data is then retrieved at a later time after equilibration.

5. MECHANICAL FAILURE AND FRACTURING IN ARGILLACEOUS ROCK ASSOCIATED WITH ABNORMAL PRESSURE

An important factor related to abnormal overpressure is the potential to cause brittle fracturing. Abnormal overpressure tends to put a rock in a brittle condition that can lead to development of permeable shear or tensile fractures. Here we review some theoretical aspects of geomechanics and rock failure and then present field observations concerning natural fracturing in argillaceous rock.

5.1 Geomechanics of Failure

The plane stress conditions in a rock can be represented on a diagram of effective normal stress versus shear stress as shown in Figure 1.

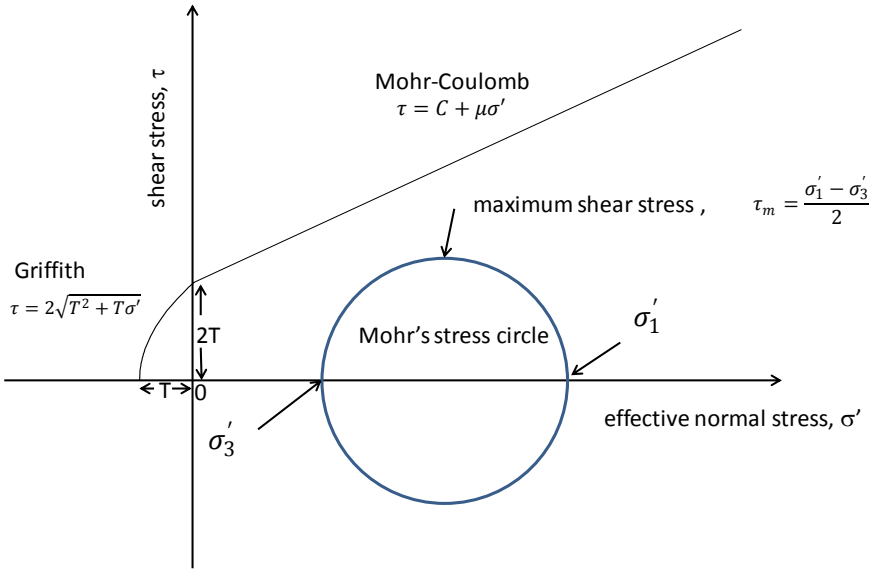

Figure 1. Mohr-Coloumb-Griffith failure curve and Mohr's stress circle.

The Mohr-Coloumb-Griffith failure curve shown in Figure 1 is a combination of the Mohr-Coloumb relationship for positive normal stress,

$$\tau = C + \mu\sigma' \tag{1}$$

where C is the cohesive strength, μ is the coefficient of internal friction, σ' is the effective normal stress, and τ is the shear stress. The failure curve under tensile stress ($\sigma_e < 0$) is given by the Griffith criterion,

$$\tau = 2\sqrt{T^2 + T\sigma'} \tag{2}$$

where T is the tensile strength (> 0).

Effective stress is the rock stress exerted by the solid framework of the rock minus the pore pressure exerted by the fluid occupying the pores. For normal stress, $\sigma' = \sigma - p$, where σ is the rock normal stress and p is the pore fluid pressure. There are a range of normal stress conditions at a given point because of the directional dependence of the rock stress. All stress conditions at a point are represented by Mohr's stress circle, with normal and shear stresses varying according to the orientation of the normal surface at that location. The peak shear stress at any location is related to the maximum and minimum normal effective stresses at that location, $\sigma_1^{'}$ and $\sigma_3^{'}$, respectively, and is given by,

$$\tau_p = \frac{\sigma_1^{'} - \sigma_3^{'}}{2} = \frac{\sigma_1 - \sigma_3}{2} \tag{3}$$

If we assume that the rock stresses are unaffected by changes in pore pressure, then shear stress is independent of pore pressure. As pore pressure increases (stress state A goes to A' and B goes to B' in Figure 2), effective stress is reduced and a stress state can contact the failure curve. As identified by Cosgrove (2001), at sufficiently high pore pressure the stress state will intersect the failure curve at a positive value of σ_e if $\tau_p > 2T$, or $\sigma_1^{'} - \sigma_3^{'} > 4T$. When the stress state intercepts the failure curve under positive normal stress (compression) conditions, the rock undergoes shear failure. When the stress state intercepts the failure curve under negative normal stress (tensile) conditions, the rock undergoes tensile failure.

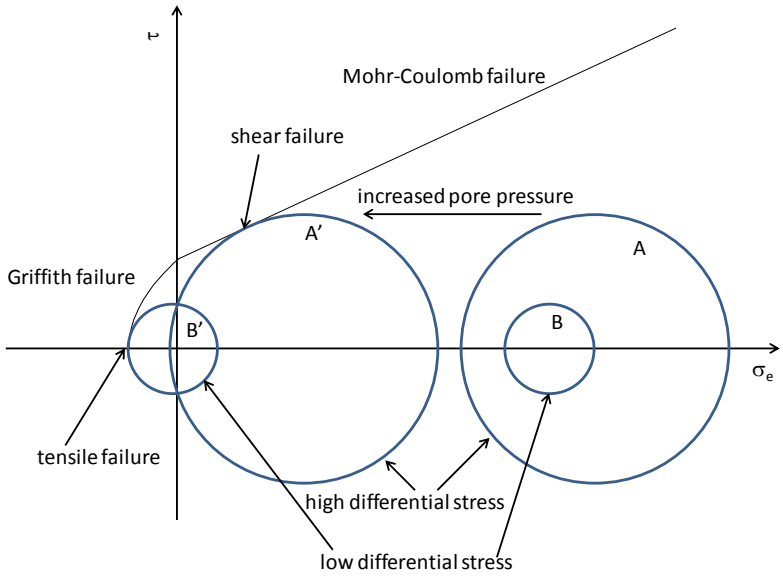

Figure 2. Shear failure induced by overpressure.

Vertical normal stress, σ_v, in a saturated rock varies linearly with depth for a homogeneous system because the weight of the overburden is proportional to depth,

$$\sigma_v = \{(1-\phi)\rho_g + \phi\rho_w\}gz \tag{4}$$

where ϕ is the porosity, ρ_g is the grain density, ρ_w is the density of water, g is gravitational acceleration, and z is depth below ground surface.

Rock stress in the presence of fluid pore pressure is governed by the effective stress, $\sigma_v^{'}$,

$$\sigma_v^{'} = \sigma_v - p \tag{5}$$

where p is the fluid pore pressure. For hydrostatic conditions, $p = \rho_w g z$. From (4), (5), and the hydrostatic pressure equation,

$$\sigma_v^{'} = (1-\phi)\left(\rho_g - \rho_w\right) g z \tag{6}$$

5.1.1 Treatment of Horizontal Stress

Horizontal stress has been found to also vary linearly with depth both for dry and saturated systems, however the rate of increase of horizontal stress with depth differs such that the ratio of horizontal to vertical stress is constant (Terzaghi and Richart, 1952; Hamouche et al., 1995). For a saturated system,

$$\frac{\sigma_h^{'}}{\sigma_v^{'}} = K_{0L} \tag{7}$$

The ratio of horizontal effective stress to vertical effective stress under conditions of zero lateral strain, K_{0L}, is called the coefficient of earth pressure at rest (Hamouche et al., 1995). Here the subscript "L", for "loading" identifies this as a coefficient for increasing vertical and horizontal stress. Cosgrove (2001) assumes the coefficient of earth pressure at rest is the same for loading and unloading processes. The coefficient has been found to be sensitive to the plasticity index and the overconsolidation ratio (Hamouche et al., 1995; Keskin et al., 2004; Shohet, 2008). The minimum horizontal stress is generally used in Equation (7) for horizontal effective stress (Hillis, 2003). For an elastic rock with no lateral strain, Hooke's law generalized to include Poisson's ratio, ν, can be used to show that,

$$K_{0L} = \frac{\nu}{1-\nu} \tag{8}$$

For the assumptions used in Figure 2, Cosgrove (2001) shows that tensile fractures will form above a threshold depth defined by the depth where $\sigma_v^{'} - \sigma_h^{'} = 4T$. Using this threshold criterion with Equations (6) and (7) gives,

$$z_{TS} = \frac{4T}{(1-K_{0L})(1-\phi)\left(\rho_g - \rho_w\right) g} \tag{9}$$

where z_{TS} is the threshold depth for tensile and shear failure. Below this depth the differential stress is too large and Mohr's stress circle, with sufficiently large pore pressure, will intercept the failure curve under positive normal stress, leading to shear failure (Figure 2).

Hillis (2003) suggests that Equation (7) should hold generally, not just for depth variations in stress at hydrostatic conditions as used by Cosgrove (2001), but also for changes in pore pressure. If K_{0L} remains constant as pore pressure changes, then the differential stress is,

$$\sigma_v^{'} - \sigma_h^{'} = \sigma_v^{'}(1 - K_{0L}) \quad (10)$$

This shows that as pore pressure increases and $\sigma_v^{'}$ decreases, the differential stress decreases and goes to zero when pore pressure equals the rock vertical stress. For $K_{0L} < 1$, the vertical effective stress is larger than the minimum horizontal effective stress, but could be smaller than the maximum horizontal effective stress. For $K_{0L} > 1$, the minimum horizontal effective stress is larger than the vertical effective stress; hence in this case the vertical effective stress is the minimum principal stress. Again assuming that the coefficient of earth pressure at rest is the same for loading and unloading, as pore pressure increases further and the vertical effective stress becomes negative, the horizontal effective stress becomes larger (less negative) than the vertical effective stress. As shown in Figure 3, the behavior of effective stress changes in response to pore pressure changes is quite different than in Figure 2. The reduction in differential stress with increase in pore pressure shrinks Mohr's stress circle causing increases in pore pressure to lead to tensile failure (Hillis, 2003; Cobbold and Rodrigues, 2007). However, decreases in pore pressure can lead to shear failure depending on the coefficient of internal friction and the initial stress conditions. Hillis (2003) and Tingay et al. (2003) provide field evidence supporting the hypothesis that vertical and horizontal effective stresses are coupled in this manner.

The impact of coupling effective stress is significant in terms of failure. Hillis (2003) indicates that this coupling is critical in preventing shear failure at lower pore pressures (such as shown in Figure 2) and allows a build-up in pore pressure before reaching tensile failure. In that Mohr's stress circle becomes smaller as pore pressure builds, tensile failure at low differential stresses are also more likely to be randomly oriented because the difference between the minimum and maximum normal effective stresses is small.

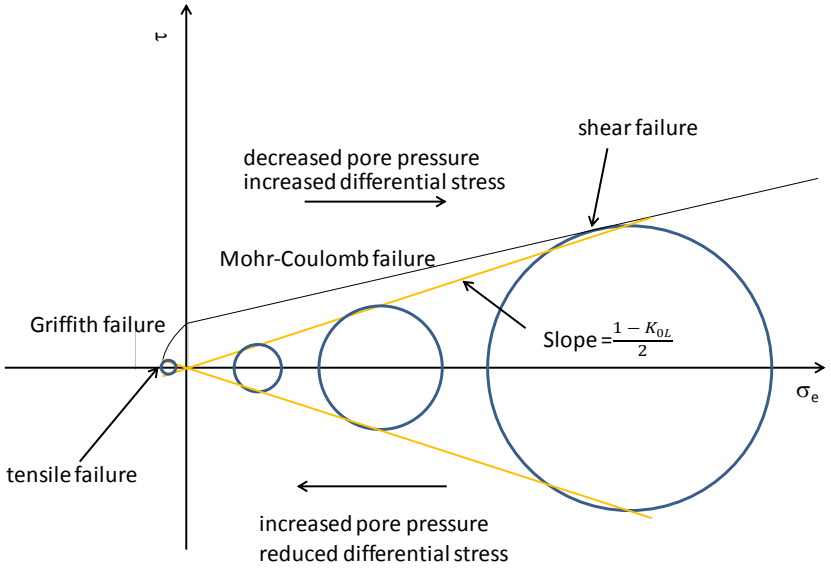

Figure 3. Effects of pore pressure on rock failure given Equation (9) for differential stress

Mertens et al. (2003) points out that differences are found between for the coefficient of earth pressure at rest (K_{0L}) during loading versus unloading, and cites Maltman (1994) for K_{0U} during unloading,

$$K_{0U} = \frac{3\nu - 1}{1 - \nu} \tag{11}$$

Although the hysteretic behavior is also noted by Wesley (2010) and Bjørlykke (2010), they suggest that unloading does not behave elastically and results in a non-linear relationship between $\sigma_h^{'}$ and $\sigma_v^{'}$. Bjørlykke (2010) presents an empirical relationship for K_{0U},

$$K_{0U} = K_{0L}\mathrm{OCR}^n \tag{12}$$

where OCR is the overconsolidation ratio and n is an empirical exponent usually between 0.6 and 0.8. A similar relationship was found for reconstituted Boston blue clay with an exponent of 0.43 (Abdulhadi et al., 2011) The overconsolidation ratio is given by,

$$\mathrm{OCR} = \frac{\sigma_{1m}^{'}}{\sigma_1^{'}} \tag{13}$$

where $\sigma_{1m}^{'}$ is the largest maximum effective normal stress experienced over time by a material element of rock, $\sigma_1^{'}$ is the maximum effective normal stress at current conditions for the material element of rock. A rock is considered normally consolidated if the overconsolidation ratio is 1, i.e., that the rock has only experienced loading. Using Equation (8) for K_{0L} and Equations (11) and (12) gives,

$$\sigma_h^{'} = \frac{\nu}{1 - \nu}\left(\sigma_{1m}^{'}\right)^n\left(\sigma_1^{'}\right)^{-n}\sigma_v^{'} \tag{14}$$

Here, $\sigma_1^{'}$ is either $\sigma_v^{'}$ or the horizontal effective stress, $\sigma_h^{'}$, noting that for zero lateral strain and isotropic properties, horizontal stresses are isotropic. If it is $\sigma_1^{'} = \sigma_v^{'}$, then,

$$\sigma_h^{'} = \frac{\nu}{1 - \nu}\left(\sigma_{1m}^{'}\right)^n\left(\sigma_v^{'}\right)^{1-n} \tag{15}$$

If it is $\sigma_1^{'} = \sigma_h^{'}$,

$$\sigma_h^{'} = \left\{\frac{\nu}{1 - \nu}\left(\sigma_{1m}^{'}\right)^n\sigma_v^{'}\right\}^{1/(1+n)} \tag{16}$$

Mertens et al. (2003) computed the trajectory of $\sigma_h^{'}$ with depth using Equations (8) and (11) and where $\sigma_v^{'}$ is given by Equation (6); Poisson's ratio is taken to be 0.4, $(1 - \phi)\rho_g + \phi\rho_w = 2000$ kg/m^3, $\rho_w = 1019$ kg/m^3, and the maximum depth is 100 m. To consider both compression (positive) and tension (negative) values of $\sigma_v^{'}$ in Equations (15) and (16), the absolute value of $\sigma_v^{'}$ is used, and $\sigma_h^{'}$ is taken to have the same sign as $\sigma_v^{'}$. A comparison of the behavior of $\sigma_h^{'}$ versus $\sigma_v^{'}$ is given in Figure 4 for the given parameters.

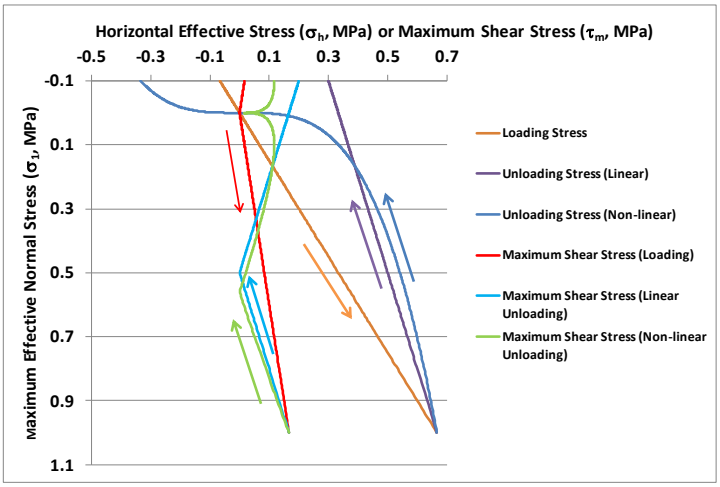

Figure 4. Horizontal and Shear Stress Paths Relative to Maximum Effective Normal Stress.

Figure 5 shows how these cases behave in terms of a Mohr-Coloumb-Griffith failure diagram with increasing pore pressure. For Figure 5, the cohesion is 0.15 MPa and the friction angle is 18°, as determined by Mertens et al. (2003). The tensile strength consistent with the magnitude of the cohesion and Griffith failure is 0.075 MPa. Differences in the treatment of K_{0L} are seen to result in different predictions for the mode of failure. Furthermore, the non-linear K_{0L} case requires about 0.317 MPa more fluid overpressure before failure occurs than the linear K_{0L} case.

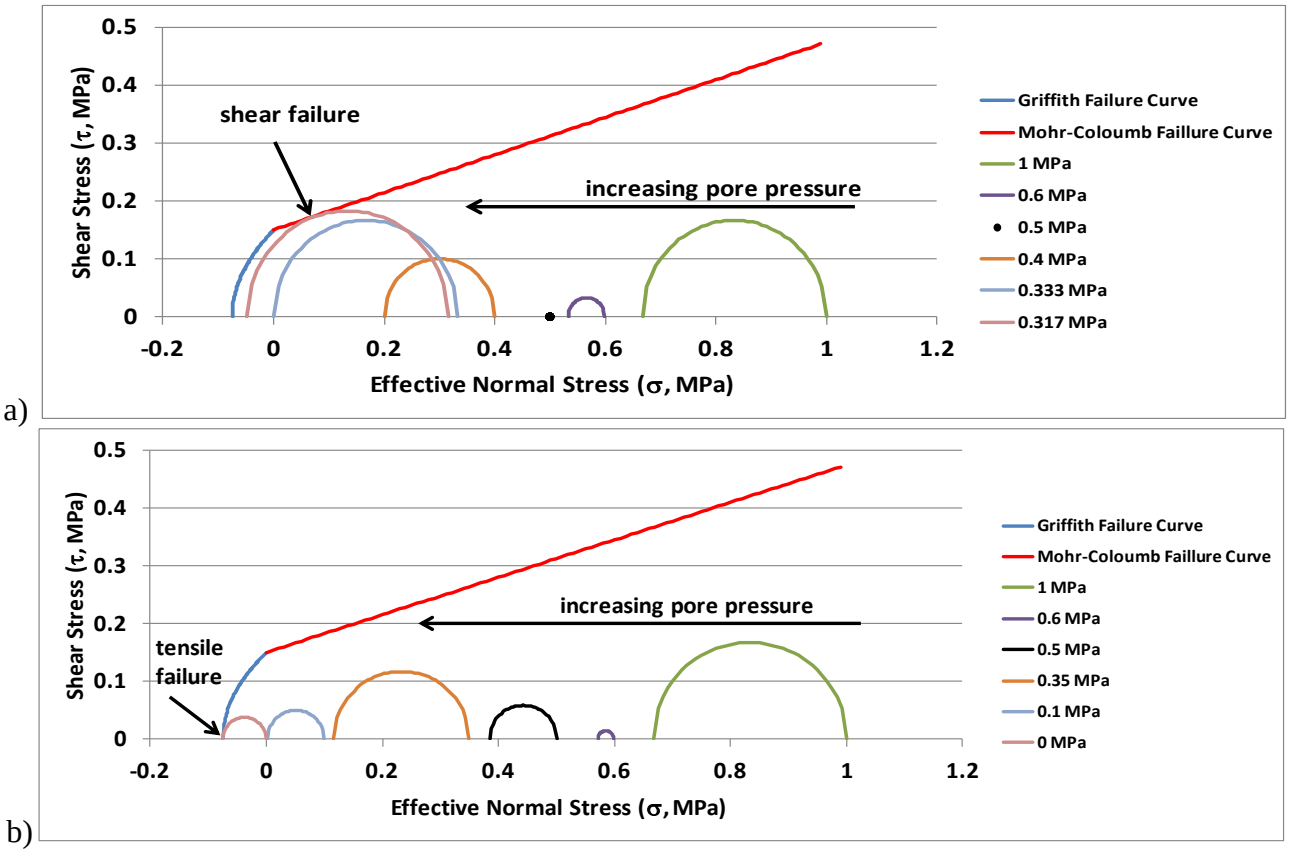

Figure 5. Mohr-Coloumb-Griffith Failure Diagrams. a) Linear $\boldsymbol{K_{0L}}$ (Equation 11); b) Non-linear $\boldsymbol{K_{0L}}$ (Equations 15 and 16).

Another aspect that impacts the consequences of shear failure concerns whether or not the failure occurs as brittle or ductile process. Failure that is brittle results in fracturing in a narrow zone with distinct shear surfaces, volumetric dilation within the fractured zone, and an increase in rock permeability. Ductile failure results in more diffuse rock deformation, volumetric contraction along the damage zone, and reduced rock permeability. Brittle and ductile failures were investigated by Ingram and Urai (1999) and Nygård et al. (2006) for argillaceous rock. These investigations found that clay rock behaves as brittle or ductile depending on the overconsolidation ratio. However, because chemical diagenesis can also affect the brittleness of a mudrock, Ingram and Urai (1999) proposed a criterion for determining the threshold between brittle and ductile behavior based on the unconsolidated compressive strength of the rock. Nygård et al. (2006) also showed in laboratory tests that brittle shear fractures can lead to enhanced rock permeability. The proposed criterion, called the brittleness index, or BRI, is,

$$\mathrm{BRI} = \frac{\mathrm{UCS}}{\mathrm{UCS_{NC}}} \tag{17}$$

where UCS is the unconfined compressive strength and $\mathrm{UCS_{NC}}$ is the unconfined compressive strength of a normally-consolidated rock at the same depth. The value of the brittleness index

corresponding to threshold brittle behavior in mudrock was determined to be 2. The unconfined compressive strength can be measured directly on core samples or estimated from measurements of seismic velocities (Ingram and Urai, 1999):

$$\frac{\log(\mathrm{UCS}) - 6.96}{2.45} = \log(V_s) = \log\left(0.86V_p - 1172\right) \tag{18}$$

where UCS is in MPa, V_s and V_p are secondary and primary seismic velocities, respectively, in m/s. The unconfined compressive strength for normally consolidated conditions can be estimated from (Ingram and Urai, 1999):

$$\mathrm{UCS_{NC}} = 0.5\sigma' \tag{19}$$

where σ' is the maximum effective normal stress at the depth of interest.

Nygård et al. (2006) developed a relationship between the overconsolidation ratio and the brittleness index:

$$\mathrm{BRI} = \mathrm{OCR}^{0.89} \tag{20}$$

where BRI is the brittleness index. The index corresponding to the threshold for brittle-ductile behavior is an overconsolidation ratio of 2.5.

5.2 Observations of Rock Failure

These results indicate that shear failure will not result in fracturing unless the current maximum effective stress is significantly less than largest maximum effective stress experienced by the rock, or alternatively if the rock has been significantly altered by cementation. Ishii et al. (2011) investigated brittle-ductile behavior for mudrock at the Horonobe underground research laboratory in Japan. The rock showed ductile behavior for a brittleness index less than 2, and a wide transition region for a brittleness index between 2 and 8 showing some fracturing but incomplete fracture connectedness limited its impacts on permeability. For a brittleness index greater than 8, the rock was strongly affected by fracture permeability. Rock that exhibits brittle behavior were found to be limited to depths less than 500 m. Similarly, studies of fault permeability at Horonobe (Ishii et al., 2010) have found that highly permeable sections formed through tensile failure are found in rock less than 400 m deep, whereas in deeper areas, faults formed through shear failure and have lower permeability. In general, the lower-permeability associated with shear failure is linked to a relationship between the brittleness index and the friction angle, φ, is (Ishii et al., 2011),

$$\mathrm{BRI} = \frac{4\cos(\varphi)}{\cos(\varphi) - 0.5} \tag{21}$$

where the coefficient of internal friction from Equation (1), $\mu = \tan(\varphi)$. Ingram and Urai (1999) present a correlation between the internal friction angle and the specific surface area, S, of mudrock:

$$\log(\varphi) = \log(35)\{1 - S/1266\} \tag{22}$$

where S is in m^2/g, suggesting that with equations (17), (18), (19), and (21), the in-situ specific surface area of a mudrock can be estimated from seismic velocities and the effective normal stress at depth.

Some additional information on permeability changes during shear failure are presented by Wong and Zhu (1999), who review experimental data concerning shear failure and interpret this data in terms of a percolation network model. Although their work did not directly address argillaceous rock, they do investigate differences in the hydrogeological behavior of shear faults for low-porosity crystalline (compact) rock as compared with more porous sedimentary rock, with porosity greater than 5%. Evidence indicates that although permeability increases are observed for dilatant (brittle) shear fracturing in compact rock, permeability has been found to actually decrease for dilatant shear fracturing in porous rock – even though rock porosity increases. The explanation provided by Wong and Zhu (1999) for this unexpected behavior is that most of the dilation occurred in the primary porosity and that fracturing was limited to disconnected localized clusters. The main impact of the fracture clusters was to increase the tortuosity of the rock, causing a decrease in rock permeability. This observation of ineffective fracture network formation by shear stress is similar to the observations at the Horonobe underground research facility in which shear failure led to poorly-connected fracture systems (Ishii et al., 2010 and 2011).

5.3 Shale-Gouge Ratio and Permeability Related to Shear Failure

One approach that has been used to evaluate the effects of shear damage in rock is to correlate the permeability of the damage zone with the shale-gouge ratio (SGR) (Yielding et al., 1997). The SGR is defined at any point along the fault as the clay volume fraction within a "window" at that location having a height equal to the throw along the fault. Therefore, SGR varies between 0 and 1. Manzocchi et al. (1999) developed a quantitative permeability relationship based on the SGR concept, given by,

$$\log(k) = -4\mathrm{SGR} - 0.25\log(D)(1-\mathrm{SGR})^5 \qquad (23)$$

where k is permeability in millidarcies, and D is the displacement along the fault. While this relationship has been developed for "faults", it has been compared with data for range of displacement distances, down to 1 mm (Manzocchi et al., 1999). It turns out that k has low sensitivity to D when SGR is greater than 0.4. This relationship has been compared with field and laboratory data and appears to provide a reasonable estimate of permeability caused by shear damage (Crawford et al., 2002, 2008). Although this relationship has been applied mainly to permeability orthogonal to the fault plane, experiments reported by Crawford et al. (2002, 2008) show agreement with this relationship for permeability along the fault plane as well. The main data set was developed for kaolinite clays, but much more limited data for illite shows permeabilities that are 3 to 4 orders of magnitude lower than those given by Equation (23). The data appear to indicate that for an SGR > 0.5, permeability effects of shear displacements are small (Crawford et al., 2008). Experiments on shale smear incorporated into shear displacement structures indicate that the mechanical properties of the clay may also play an important role (Schmatz et al., 2010).

6. NATURAL FRACTURES IN ARGILLACEOUS ROCK

Only a few deep-bedrock argillaceous formations have been extensively characterized for hydrogeologic purposes (Cherry et al., 2006). In the U.S. these are the Pierre Shale (Neuzil, 1986) and the Maquoketa Formation (Eaton et al., 2007). Worldwide, some deep argillaceous formations are being intensively studied in Switzerland (Opalinus Clay), Belgium (Boom Clay), France (Callovo-Oxfordian Clay and Toarcian argillites), and Japan (Koetoi and Wakkanai Formations) for nuclear waste disposal. Natural fractures in deeper bedrock argillaceous formations have not received a much attention because they have been found to generally have low permeability (Gautschi, 2001; Gautschi et al., 2004), although at larger scales, may be more important (Neuzil, 1994, Eaton et al., 2007).

More recently, argillaceous rock have received more attention from the petroleum industry regarding the recovery of petroleum fluids from shales. The effects of natural fractures in these formations have only recently been investigated (Gale and Holder, 2010). Induced hydraulic fractures have been found to interact with existing natural fractures in shales leading to development of enhanced permeability (Loucks et al., 2012; Gale et al., 2007; Gale and Holder, 2010). Shales of interest for methane thermogenesis are generally deep, below 2 km, and the fractures are generally found to be cemented, primarily by calcite (Gale and Holder, 2010; Demirbas, 2010). However, unmineralized fractures may be important in shallow mudstones where temperatures are too low for cement growth (Gale and Holder, 2010).

6.1 Observations of Natural Fractures in Argillaceous Rock

A presentation of evidence suggesting that transient, episodic hydraulic fracturing had occurred in the Mercia Mudstone Group was given by Cosgrove (2001). These mid-to-late Triassic mudstones consist of illite, chlorite, mixed-layer, and smectite clays as well as quartz, calcium and magnesium carbonates, calcium sulfates, micas, iron oxides, and halite (Hobbs et al., 2002). Following deposition, the formation was subjected to burial during an approximately 150 million-year period of tectonic extension. The maximum burial depth was about 2.4 km. At that point there was a tectonic inversion resulting in compression and uplift over the next 100 million years to the present day, where in some locations the Mercia Mudstone is present at the ground surface. At some of the outcrop locations, the Mercia Mudstone shows signs of hydraulic fracture and fluid movement through fractures as evidenced by deposition of sand or gypsum precipitate that preserved the fractures. During the extensional period the higher vertical stress leads to vertical fractures, opening in the direction of the minimum horizontal stress. Vertical fractures were preserved by mobilization and filling of at least some of these fractures with sand. Later during uplift, with high lateral stress caused by tectonic compression, fractures preferentially form in the horizontal direction against the relatively smaller vertical stress. Sub-horizontal fractures have been preserved by gypsum precipitate. The cross-cutting relationships between the horizontal and vertical fractures show that the horizontal fractures occurred later in the process. Furthermore, the low-temperature conditions required for the formation of gypsum from anhydrite limit the depth at which gypsum-filled fractures could have formed during uplift. Observations of these later episodes of fracturing were only seen in the horizons that contained anhydrite, which could mean that fracturing in other horizons occurred but were not preserved, or could mean that hydration of anhydrite to gypsum played a role in these more recent fractures. The conclusions reached by Cosgrove (2001) may be summarized as (1) sedimentary basin sediments are subjected to hydraulic fracturing as a result of a build-up of excess, abnormal pressure caused by burial

compaction and tectonic stress; (2) fluids are discharged from the sediments through the hydraulic fractures to relieve the excess pressure; (3) hydraulic fractures close after pressure is relieved and evidence of their existence is lost if not preserved by some infilling material; and (4) the process of hydraulic fracturing can occur at various stages of basin evolution, during both burial and uplift.

A similar process of episodic transient flow through hydraulic fractures in argillaceous rock caused by abnormal overpressure is proposed by Horseman and Harrington (1996). Because of the greater capacity for gas to store energy in compression, they find that episodic flow of gasses may be common. Seabed pockmarks and migration of oil and gas are cited as evidence for such phenomena.

A somewhat different process of hydraulic fracturing of the Ieper Clay as a result of abnormal overpressure is reported by Henriet and De Baptist (1996). Burial compaction is identified as the cause of overpressure and significant undercompaction of the clay. However in this case, buoyancy caused by undercompaction of the clay led to a gravitational Raleigh-Taylor instability of the entire clay body, leading to sediment flow lubricated by the strong overpressure and reduced effective stresses. As for the case described by Cosgrove (2001), the pressure release and fluid flow is a transient process that ends when the sediment is further compacted and pressure is relieved by flow through the fractures.

Beaudoin (1998) reported that fractures in well-stratified Albian and Aptian marls near Bevons in the south of France are preserved by sedimentary sand dykes. The narrow sedimentary sand dykes are found to be from 1cm to 1 m thick and up to 250 m long. Beaudoin (1998) concludes that this case provides further evidence that early fracturing in marls may be expected.

Observations from shales containing natural gas or oil indicate that natural opening-mode fractures common in present in most mudrocks and act as weak planes that reactivate during hydraulic fracturing (Gale and Holder, 2010). Smaller natural fractures were found to be sealed but larger fractures can remain open. The crossover size at which fractures are found to be sealed or open is a function of the fracture opening rate and the rate cement (e.g., silica or calcite) deposition in the fractures. Larger fractures that are open tend to occur in clusters with cluster spacing related to the mechanical layer thickness and a subcritical index, n, that relates to the velocity of subcritical fracture propagation (Olson, 2004).

Petroleum reservoir leakage through natural fractures in argillaceous caprocks can occur as a result of overpressure caused by the height of the gas and oil column trapped (Brown, 1999). This is also evidenced by the fact that petroleum reservoirs frequently have closure heights that exceed the seal strength height – a sign that caprock leakage has stopped the accumulation of oil and gas (Sales, 1997).

6.2 Flow and Transport through Hydraulic Fractures in Response to Abnormal Overpressure

The results presented here have indicated that evidence for hydraulic fracturing and fluid flow associated with abnormal pressure in argillaceous rocks during basin evolution may be quite limited. Another way to evaluate the role of fluid flow and other transport mechanisms in low-permeability rock is to analyze natural tracer distributions in pore waters. Three sets of

information are required to analyze natural tracer data in terms of transport processes (Mazurek et al., 2011): (1) spatial distribution of tracer concentrations, (2) formation properties that are relevant for solute transport, and (3) the palaeo-hydrogeological framework to constrain conditions at the system boundaries over time. Analyses of transport processes in argillaceous formations using natural tracer data at nine locations are presented by Mazurek et al. (2011). The analyses found diffusion-dominated transport could explain the data in all cases and in several cases significant advective transport could be excluded; however, in some cases the effects of advective transport at a level comparable to diffusive transport could not be definitively excluded. For the analyses performed by Mazurek et al. (2011) vertical advection is assumed to be constant over time. The possibility that transient flow through limited, discrete pathways was not included. For transient flow processes such a pressure relief flow through a hydrofracture, tracer diffusion during the time period after the event would make it difficult to distinguish from the initial tracer concentration (Mazurek et al., 2011). Calculations are presented here to consider how tracer concentrations are affected by transient flow and transport associated with abnormal pressure and hydrofracture for a hypothetical argillaceous formation.

6.2.1 Model Description

The model domain and properties are shown in Figure 6. A situation in which a single hydrofracture penetrates a low-permeability argillaceous rock is modeled, using symmetry no-flow and no transport boundary conditions along the fracture centerline on the left-hand-side boundary and at the midplane between hydrofractures on the right-hand side boundary. The fracture spacing is 10 m for a 100-m thick argillaceous rock. A 100-m thick aquifer that is present below the argillaceous formation. A constant-pressure boundary is used at the top of the argillaceous formation, representing an overlying permeable aquifer. Overpressure conditions are assumed in the argillaceous rock and the underlying aquifer at the time of hydrofracture, with normally-pressured conditions in the overlying zone.

For this analysis, simplifying assumptions are used to set-up the hydrofracture geometry. Key features of the hydrofracture geometry are the fracture spacing and permeability, however, predicting these features of hydrofractures are subject to significant uncertainty. A more fundamental treatment of hydrofracture development requires a combined treatment of hydro-mechanical and fracture damage processes.

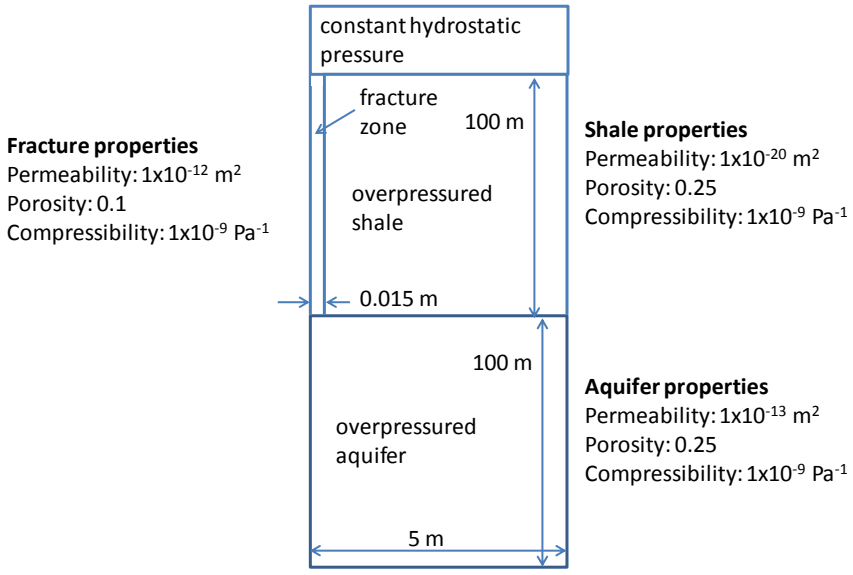

Figure 6. Domain diagram for hydrofracture pressure relief flow and transport.

The rock properties given in Figure 6 are loosely based on values for the Opalinus Clay at Mont Terri and Boom Clay at Mol (Houseworth and Persoff, 2012).

The aquifer and shale are initially overpressured by 2 MPa and the top of the shale is at a depth of 500 m, and the zone above the shale has a fixed hydrostatic pressure of 4.9 MPa. The overpressure is roughly based on a saturated bulk density of 2450 kg/m^3 giving a total overburden pressure of about 12 MPa at the top of the shale and the coefficient of earth pressure at rest given by Equation (8). A Poisson's ratio of 0.25 and tensile strength of zero is used for the shale. This information can be used to determine the lateral effective stress. The lateral effective stress plus the tensile strength is the fluid overpressure target for generating a hydraulic fracture.

A tracer mass is distributed throughout the aquifer that begins to move by advection and diffusion at time zero when the hydrofracture opens. The tracer mass diffusion coefficient used is 5×10^{-11} m^2/s, which is based on Mazurek et al. (2011) for the Opalinus Clay at Mont Terri. The calculation is carried out using TOUGH2-EOS7R (Oldenburg and Pruess, 1995).

A refined grid is used around the fracture because studies reported by Liu et al. (2012) show that fine gridding is needed to accurately capture fracture-matrix diffusive transport processes. The grid uses discretization shown in Table 2. The fracture zone has a half-width of 0.015 m and the first matrix grid elements along the fracture have a lateral dimension of 0.002 m. While the vertical dimension for most of the cells is 0.5 m, fine gridding is used again at the top and bottom of the shale and top of the aquifer to more accurately capture diffusive exchange.

Table 2. Grid dimensions.

Lateral dimension (m), left to right across domain – shale and aquifer	0.015 (fracture) →	0.002	0.004	0.008	0.016	0.032	0.064	0.128	0.256	0.512	0.963	1 (3)	
Vertical dimension (m) top to bottom across shale	0.002	0.004	0.008	0.016	0.032	0.064	0.128	0.256	0.490 →	0.5 (196) ↓			
	0.490 ←	0.256	0.128	0.064	0.032	0.016	0.008	0.004	0.002 ←				
Vertical dimension (m) top to bottom across aquifer	0.002 →	0.004	0.008	0.016	0.032	0.064	0.128	0.256	0.490	1 (9)	2 (5)	5 (2)	10 (7) →

Note: numbers in parentheses represent the number of adjacent cell dimensions that are repeated. Arrows denote direction of top to bottom and left to right.

6.2.2 Fracture Flow and Pressure Distributions

The initial pressure distribution is shown in Figure 7, where the top of the shale is taken to be at 500 m total depth.

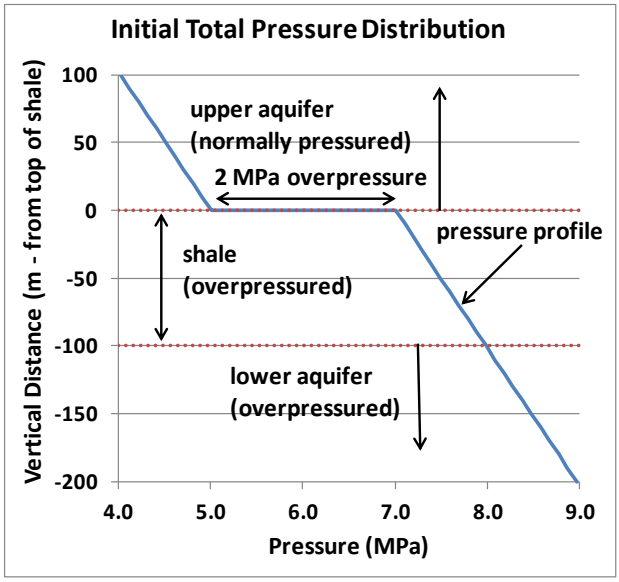

Figure 7. Initial pressure distribution.

The fluid flow from the fracture into the overlying formation is shown in Figure 8. There are three distinct periods in the fracture flow rate that can be interpreted through the dynamic pressure distribution, also shown in Figure 8 at several points in time. The dynamic pressure is the total pressure minus the hydrostatic pressure, which is the same as fluid specific weight of water times the piezometric head. This way of displaying pressure isolates the pressure variations associated with fluid movement.

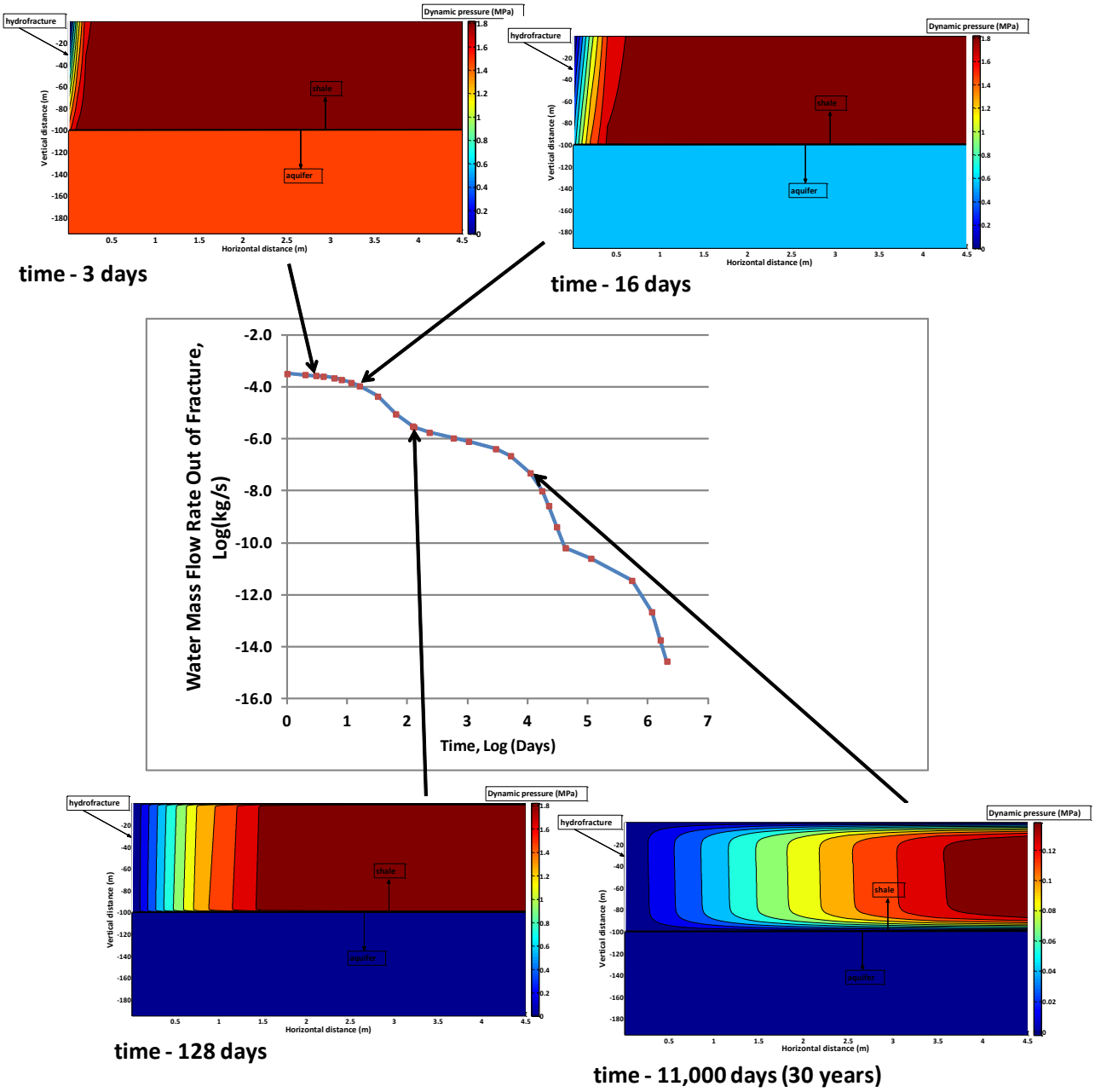

Figure 8. Flow rate in the fracture at the top of the shale and piezometric head evolution during depressurization. Note that the pressure contour plots are highly compressed in the vertical direction.

During the initial flow period that lasts approximately four months, the underlying aquifer pressure is being rapidly depleted. Flow through the aquifer to the fracture causes only minor pressure loss because of the high permeability of the aquifer. Therefore, the aquifer acts like a homogeneous "pressure tank" that depletes as flow is discharged. Flow rates along the fracture during the initial period are nearly constant spatially because most of the flow enters the fracture from the aquifer and is discharged at the top of the shale into the overlying formation. As can be seen by 128 days, there is little excess pressure remaining in the aquifer. However, the further decline in the flow rate is moderated by the much slower decline in pressure for the shale. The shale pressure depletion period lasts about 30 years. During this period, fracture flow is supplied mainly by lateral flow from the shale. The flow rate along the fracture builds up from the base to the top of the shale. During the final period beyond 30 years, very low flow rates are supplied by both the aquifer and the shale as the remnants of excess pressure dissipate.

6.2.3 Solute Transport from the Aquifer

The aquifer may contain solutes that distinguish the aquifer pore water from the shale pore water. One example of this presented in Mazurek et al. (2011) is for the Opalinus Clay. Both bounding aquifers and the Opalinus clay were deposited in seawater such that the initial pore waters contained high levels of chloride relative to meteoric water. After a long period of burial and uplift, the upper aquifer was exposed at the surface to meteoric water inflow which caused a sharp decline in chloride concentration in the aquifer. Chloride levels in the shale pore water remained high because of the extremely low flow rates that occur in the low-permeability shale. However, the change in chloride concentrations at the shale-aquifer boundary initiated chloride diffusion out of the shale which is ongoing still at this time. A similar change in pore-water chemistry occurred in the lower aquifer as a result of erosion and intrusion of meteoric water several million years after the change in the upper aquifer.

In the calculation performed here, an initial concentration of solute is assigned to the aquifer with zero concentration in the shale as an initial condition. For chloride, it would be more likely to have initially high concentrations in the shale and low concentration the aquifer as discussed above. However, this could represent a case in which a recent exposure of the lower aquifer to meteoric recharge carries a higher concentration of some tracer (e.g., isotopes) than present in the shale or upper aquifer. Solute is transported by advection and diffusion through the domain in response to concentration gradients and the hydrofracture-induced flow patterns. The pore diffusion coefficient used, D, is 1×10^{-11} m^2/s.

Figure 9 shows the evolution of a solute initially present in the aquifer as it spreads into the shale through diffusion and advection and is also discharged into the overlying formation. At early times during flow through the hydrofracture, solute from the aquifer is confined to a very narrow zone around the fracture. In Figure 9, after 308 years, a relative concentration of 0.01 of aquifer solute has moved about 0.5 m from the fracture. At longer times, only lower solute concentrations occupy large sections of the shale. By 19,000 years, lateral variations in the solute concentration pattern associated with the hydrofracture flow have been lost. However, there is a residual concentration on the order of 0.001 remaining throughout most of the shale. Note that the transport of solute from the fracture across the shale occurs despite the advective flow pattern that would tend to

move solute back towards the fracture. Most of the solute redistribution laterally occurs during the third stage of the flow event where solute transport is dominated by diffusion.

The one-dimensional solute concentration profiles along the hydrofracture, also given in Figure 9, show a comparison of these profiles with an analytical solution for one-dimensional diffusion. At early times, the analytical solution is closely approximated by,

$$c = \frac{1}{2} - \frac{1}{2}\,\mathrm{erf}\left(\frac{z + 100}{\sqrt{2Dt}}\right) \tag{24}$$

where c is the relative concentration and D is the diffusion coefficient. As can be seen, the solute concentration for the more complex numerical solution is closely matched by the analytical solution at high concentrations, and deviates from this only for solute concentrations of 0.03 at 308 years. The solutions continue to converge until the profile is one-dimensional by 19,901 years and the residual discrepancy between these solutions is limited to relative concentrations on the order of 0.001. This is a test of the system.

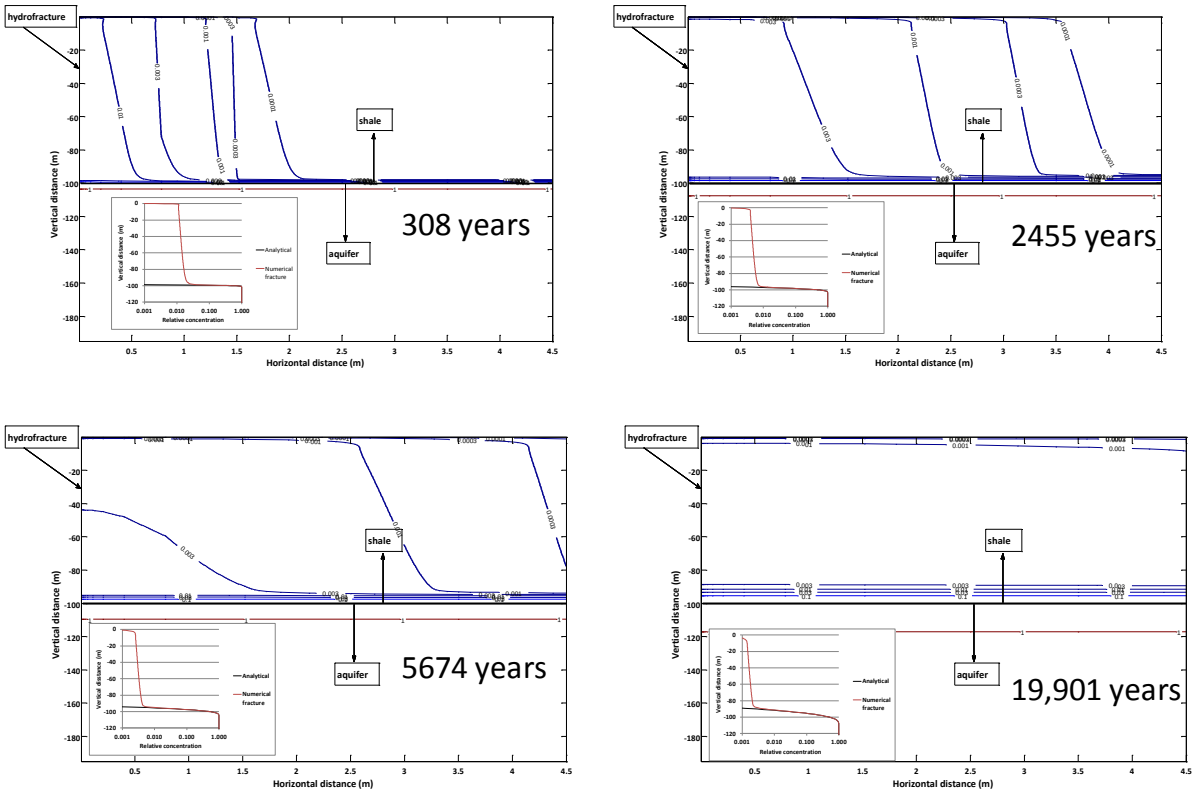

Figure 9. Relative concentration contours of aquifer tracer at four times after initiating hydrofracture flow. Note that hydrofracture flow has virtually ceased even at the first time shown here (308 years – see also Figure 8). Inset with each contour plot shows vertical concentration distribution along fracture along with analytical one-dimensional diffusion solution.

Therefore, the main long-term effect of solute introduced is to increase the apparent background concentration of solute from the aquifer in a process that could be described as "hydrofracture injection".

6.2.4 Hydrofracture Injection

Given the behavior of solute transport through hydrofractures, one possible way to simplify the analysis of hydrofracture solute movement is to neglect the transient transport that occurs as a result of the hydrofracture and treat the effects as a time-dependent, distributed source-sink term. As a first approximation, the source-sink term could be treated as proportional to the difference between the local solute concentration in the shale pore water, c, and the solute concentration of the injected aquifer water, c_{aq}, through an empirical rate constant, $\alpha(t)$. The resulting solute transport equation is,

$$\frac{\partial c}{\partial t} + \alpha(t)\left(c - c_{aq}\right) = D\frac{\partial^2 c}{\partial z^2} \tag{25}$$

This equation is applied to a finite, one-dimensional domain from $z = 0$ to $z = \ell$. The specific case to be examined here is $c(0,t) = c(\ell,t) = 0$, $c_{aq} = 0$, and $c(z,0) = c_0$. This implies that at some time in the past ($t = 0$ in this model), solute concentrations in both upper and lower aquifers decreased from c_0 to zero. A non-dimensional form for (25) is,

$$\frac{\partial \hat{c}}{\partial \tau} = \frac{\partial^2 \hat{c}}{\partial \xi^2} \tag{26}$$

with $\hat{c}(0,\tau) = 0$; $\hat{c}(1,\tau) = 0$; $\hat{c}(\xi,0) = 1$, where $\tau = \frac{Dt}{\ell^2}$, $\xi = \frac{z}{\ell}$, $R(t) = \frac{\alpha(t)D}{\ell^2}$, and $\hat{c} = \frac{c}{c_0}\exp\left(\int_0^t R(\tau)\,d\tau\right)$. The solution is obtained from Carslaw and Jaeger (1959, Section 3.3),

$$c(\xi,\tau) = \frac{4}{\pi}\left\{c_0 \exp\left(-\int_0^t R(\tau)\,d\tau\right)\right\}\sum_{n=0}^{\infty}\left[\frac{\exp\{-(2n+1)^2\pi^2\tau\}}{2n+1}\sin\{(2n+1)\pi\xi\}\right] \tag{27}$$

The solution is identical to a case without direct injection ($R = 0$), if the initial concentration of solute in the shale pore water is taken to be $c_0\exp\left(-\int_0^t R(\tau)\,d\tau\right)$. Because the initial concentration in the shale pore water can only be estimated indirectly, it may be difficult to assess the relative contributions of direct injection and diffusive transport based on solute profiles.

6.2.5 Solute Transport from the Shale

The hydrofracture flow process can also displace solutes present in the shale. The scenario presented in Figure 10 is for solute present in the first matrix grid cell immediately adjacent to the fracture at a vertical position in the middle of the shale (see Table 2). The same flow rate graph through the fracture is plotted here as shown in Figure 8. What is seen is that tracer located close to the fracture can be rapidly mobilized and discharged from the shale. Nearly the entire tracer

mobilized by hydrofracture flow occurs during the first phase of the flow profile, roughly during the first 100 days. Because of the quick decline in flow rate, the only tracer that can be effectively discharged by this mechanism is tracer close enough to the fracture so the solute can diffuse to the fracture over this time period. Although there is matrix flow towards the fracture, this mechanism is weak relative to diffusion. The length scale corresponding to diffusion over a 100-day period is $\sim\sqrt{Dt}$, or about 0.01 m. Therefore, solute within the shale impacted by hydrofracture flow tends to be restricted to extremely narrow regions in the immediate vicinity of the fractures. This result could change if the hydrofracture remains open for extended periods (for example if filled with mobilized sand) and other, longer-term driving forces for flow across the shale were present.

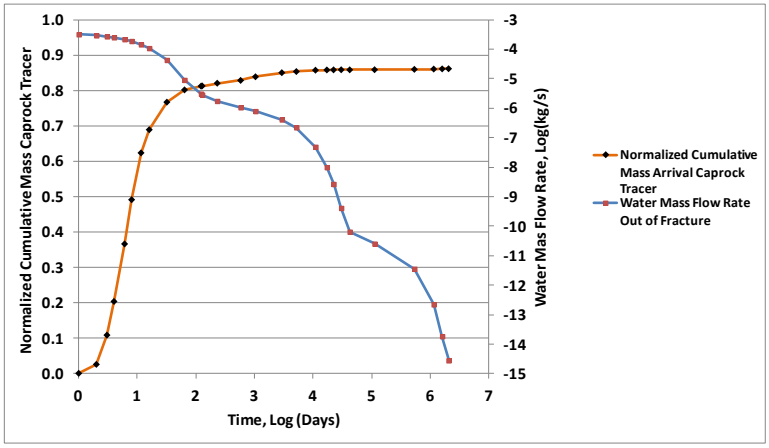

Figure 10. Tracer transport from matrix cell adjacent to fracture at mid-depth in the shale to overlying aquifer.

7. CONCLUSIONS

Abnormal pressure is commonly found in associated with low-permeability horizons such as argillaceous rock. Abnormal pressure can result from a wide variety of mechanisms related to normal diagenetic processes of the argillaceous rock itself or from external factors such as tectonic compression. Regardless of the source of pressure, the low permeability characteristic of argillaceous rock cannot readily transmit and dissipate excess pressure resulting in the potential for a build-up of abnormal pressure.

Mechanical damage caused by abnormal pressure is more likely to result in overconsolidated conditions and the resulting brittle fracturing conditions because of the general lowering of effective stress that accompanies abnormal pressure. Empirical relationships between vertical and horizontal rock stress appear to reduce differential stress under conditions of abnormal pressure, which allows for a greater build-up of abnormal pressure and increase the likelihood of tensile fracturing than shear fracturing. Several aspects of shear fracturing, ductile versus brittle conditions, and shale smear during shear fracturing tend to reduce the hydrogeologic effects of shear fractures, although permeability enhancement in shear fractures has also been demonstrated. By contrast, tensile fractures resulting from abnormal pressure, also called hydrofractures, are expected to enhance permeability for as long as the fractures remain open.

Evidence of natural hydrofracturing in shales exists and shows that flow and transport can occur through hydrofractures. In cases where such transport processes lead to some type of mineral deposition in the fractures, evidence of the hydrofracture process can be preserved. If hydrofractures are not preserved by such deposition, the evidence for such fracturing may be absent. Consideration of flow and transport in response to hydrofracturing for an overpressured aquifer and overlying shale shows that the flow event occurs in three stages. The first flow stage results in rapid depressurization of the underlying permeable aquifer. The second flow stage is dominated by depressurization of the shale. The final flow stage is a combination of remnant excess pressure in the shale and aquifer. Solute present in the aquifer at concentrations that distinguish it from the shale pore water invades the shale along the fracture and disperses laterally between hydrofractures by diffusive transport. The ultimate solute concentration distribution returns to a vertical one-dimensional profile caused by large-scale vertical solute diffusion. While diffusive transport erases specific patterns associated with hydrofracture transport, the apparent background solute concentration is shifted across the shale in a process termed hydrofracture injection.

The rapid transient flow characteristic of hydrofracture depressurization during the first flow stage means that transport of any solutes present in the shale by this flow is restricted to solutes that are located in the immediate vicinity of a hydrofracture. The second and third flow stages appear to be too weak to significantly impact solute transport. Solute that lies within a narrow region close to a hydrofracture can be rapidly transported from the shale to overlying aquifers over a timeframe of days but solute present throughout most of the shale away from the hydrofractures will not be affected significantly.

These findings suggest that it is important to characterize the mechanical characteristics of the formation as well as potential sources of abnormal pressure when selecting sites for radioactive waste disposal. Mechanical characteristics are affected by current stress conditions, mineralogy, and diagenetic history. Assessing the past behavior of an argillaceous formation with respect to hydrofracture occurrence is problematic because of fracture self-sealing and clues left by tracer transport may be difficult to identify. However, a shift in the background concentration from expected levels may be an indication of such activity. Hydrofracture flow and transport mechanisms need to be further investigated for potential impacts on performance assessment.

8. ACKNOWLEDGEMENTS

Funding for this work was provided by the Used Fuel Disposition Campaign, Office of Nuclear Energy, of the U.S. Department of Energy under Contract Number DE-AC02-05CH11231 with Berkeley Lab. I would like to thank Patrick Dobson and Jonny Rutqvist for their helpful review comments.

9. REFERENCES

Abdulhadi, N.O., J.T. Germaine, and A.J. Whittle. 2011. Experimental Study of Wellbore Instability in Clays, Journal of Geotechnical and Geoenvironmental Engineering, August 2011. pp. 766-776.

Altaner, S.P. 1986. Comparison of Rates of Smectite Illitization with Rates of K-Feldspar Dissolution, Clays and Clay Minerals, v. 34, no. 5, pp. 608-611.

Aplin, A.C., and J.H.S. Macquaker, 2011. Mudstone diversity: Origin and implications for source, seal, and reservoir properties in petroleum systems, AAPG Bulletin, v. 95, no. 12, pp. 2031–2059.

Arnould, M. 2006. Discontinuity Networks in Mudstones: A Geological Approach - Implications for Radioactive Wastes Isolation in Deep Geological Formations in Belgium, France, Switzerland, Bulletin of Engineering Geology and the Environment, v. 65, pp. 413–422.

Bain, J.A. 1971. A Plasticity Chart as an Aid to the Identification and Assessment of Industrial Clays, Clay Minerals v. 9, pp. 1-17.

Beaudoin, B. 1998. Early Fractures Record in Argillaceous Formations: Sedimentary Dykes and Nodules, from Detection of Structural and Sedimentary Heterogeneities and Discontinuities within Argillaceous Formations, Co-ordinating Group on Site Evaluation and Design of Experiments for Radioactive Waste Disposal (SEDE), Working Group on Measurement and Physical Understanding of Groundwater Flow through Argillaceous Media (the "Clay Club"), Synthesis and Compilation of Abstracts "Clay Club" Topical Session Brussels, Belgium, 3 June 1998, Nuclear Energy Agency Committee on Radioactive Waste Management.

Belitz, K., and J. Bredehoeft, 1986. Comment and Reply on “Safe disposal of toxic radioactive liquid wastes”, Geology, March 1986, pp. 266-267.

Bjørlykke, K. 2010. Petroleum Geoscience – From Sedimentary Environments to Rock Physics, Springer Verlag.

Boles, J.R., and S.G. Franks, 1979. Clay Diagenesis in Wilcox Sandstones of Southwest Texas: Implications of Smectite Diagenesis on Sandstone Cementation, Journal of Sedimentary Petrology, v. 49, no. 1, pp. 55-70.

Bredehoeft, J.D., 1965. The Drill-Stem Test: The Petroleum Industry’s Deep-Well Pumping Test, Ground Water, v. 3 no. 3.

Brown, A.A., 1999. Predicting Preservation and Destruction of Accumulations, Chapter 11 from Treatise of Petroleum Geology/Handbook of Petroleum Geology: Exploring for Oil and Gas Traps, Pages 11-1 - 11-30, Edited by Edward A. Beaumont and Norman H. Foster.

Brown, A., 2003. Improved Interpretation of Wireline Pressure Data, AAPG Bulletin, v. 87, no. 2, pp. 295–311.

Carslaw, H.S., and J.C. Jaeger, 1959, Conduction of Heat in Solids, Oxford University Press.

Chapman, R.E., 1972. Clays with Abnormal Interstitial Fluid Pressures, AAPG Bulletin, v. 56, no. 4 pp. 790-795.

Cherry, J.A., B.L. Parker, K.R. Bradbury, T.T. Eaton, M.G . Gotkowitz, D.J. Hart, and M. Borchardt. 2006. Contaminant Transport through Aquitards : A State-of-the-Science Review. Denver, Colorado: American Water Works Association Research Foundation.

Cobbold, P.R., and N. Rodrigues, 2007. Seepage Forces, Important Factors in the Formation of Horizontal Hydraulic Fractures and Bedding-Parallel Fibrous Veins ('Beef' and 'Cone-in-Cone'), Geofluids v. 7, pp. 313–322.

Colten-Bradley, V.A., 1987. Role of Pressure in Smectite Dehydration—Effects on Geopressure and Smectite-to-Illite Transformation, AAPG, v. 71, no. 1 pp. 1414-1427.

Cosgrove, J.W., 2001. Hydraulic Fracturing during the Formation and Deformation of a Basin: A Factor in the Dewatering of Low-Permeability Sediments, AAPG Bulletin, v. 85, no. 4, pp. 737–748.

Crawford, B.R., R.D. Myers, A. Woronow, D.R. Faulkner, and E.H. Rutter, Porosity-permeability Relationships in Clay-bearing Fault Gouge, SPE/ISRM 78214, SPE/ISRM Rock Mechanics Conference, Irving, Texas, 20-23 October 2002.

Crawford, B.R., D.R. Faulkner, and E.H. Rutter, 2008. Strength, Porosity, and Permeability Development During Hydrostatic and Shear Loading of Synthetic Quartz-Clay Fault Gouge, 14 pp.

Demirbas, A., 2010. Methane Gas Hydrate, Springer-Verlag London Limited.

Dugan, B., P.B. Flemings, D.L. Olgaard, and M.J. Gooch, 2003. Consolidation, Effective Stress, and Fluid Pressure of Sediments from ODP Site 1073, US Mid-Atlantic Continental Slope, Earth and Planetary Science Letters v. 215, pp. 13-26.

Eaton, T.T., M.P. Anderson, and K.R. Bradbury, 2007. Fracture Control of Ground Water Flow and Water Chemistry in a Rock Aquitard, Ground Water, v. 45, no. 5, pp. 601-615.

Elie, M., and M. Mazurek, 2008. Biomarker Transformations as Constraints for the Depositional Environment and for Maximum Temperatures during Burial of Opalinus Clay and Posidonia Shale in Northern Switzerland, Applied Geochemistry, v. 23, pp. 3337–3354.

Fertl W.H., and G.V. Chilingarian, 1987. Abnormal Formation Pressures and their Detection by Pulsed Neutron Capture Logs, Journal of Petroleum Science and Engineering, v. 1, pp. 23-38.

Gale, J.F.W., R.M. Reed, and J. Holder, 2007. Natural fractures in the Barnett Shale and their importance for hydraulic fracture treatments, AAPG Bulletin, v. 91, no. 4, pp. 603–622.

Gale, J.F.W. and J. Holder, 2010. Natural Fractures in Some US Shales and their Importance for Gas Production, from B.A. Vining and S.C. Pickering, (eds) Petroleum Geology: From Mature Basins to New Frontiers – Proceedings of the 7th Petroleum Geology Conference, pp. 1131–1140.

Gautschi, A., 2001. Hydrogeology of a Fractured Shale (Opalinus Clay): Implications for Deep Geological Disposal of Radioactive Wastes, Hydrogeology Journal v. 9, pp. 97–107.

Gautschi, A., A. Lambert, and P. Zuidema, 2004. Project Opalinus Clay - Geoscientific Basis for the Demonstration of Feasibility of Disposal (*Entsorgungsnachweis*) for SF, Vitrified HLW and Long-Lived ILW in Switzerland, Mat. Res. Soc. Symp. Proc. Vol. 807, pp. 1-6.

Gonçalvès, J., S. Violette, and J. Wendling, 2004. Analytical and Numerical Solutions for Alternative Overpressuring Processes: Application to the Callovo-Oxfordian Sedimentary Sequence in the Paris Basin, France, Journal of Geophysical Research, v. 109, 14 pp.

Gough, D.I., and W.I. Gough, 1987. Stress Near the Surface of the Earth, Annual Review of Earth and Planetary Sciences, pp. 545-566.

Guggenheim, S., and R.T. Martin, 1995. Definition of Clay and Clay Mineral: Joint Report of the AIPEA Nomenclature and CMS Nomenclature Committees, Clays and Clay Minerals, Vol. 43, No. 2, pp. 255-256.

Hamouche, K.K., S. Leroueil, M. Roy, and A.J. Lutenegger, 1995. In Situ Evaluation of K_0 in Eastern Canada Clays, Canadian Geotechnical Journal, v. 32, pp. 677-688.

Hartzell, S.H. and J.N. Brune, 1977. Source Parameters for the January 1975 Brawley- Imperial Valley Earthquake Swarm, Pageoph, v. 115, pp. 333-355.

Hay, W.W., A. Migdisov, A.N. Balukhovsky, C.N. Wold, S. Flögel, E. Söding, 2006. Evaporites and the Salinity of the Ocean During the Phanerozoic: Implications for Climate, Ocean Circulation and Life, Palaeogeography, Palaeoclimatology, Palaeoecology v. 240, pp. 3–46.

Henriet, J.P., and M. De Baptist, 1996. Fracturation and Intraformational Faulting of the Ieper Clay: Evidence for a Major Palaeo-flow Event, from Fluid Flow through Faults and Fractures in Argillaceous Formations, A Joint NEA/EC Workshop, Berne, Switzerland, June 10-12, 1996.

Hillis, R.R., 2003. Pore Pressure/Stress Coupling and its Implication for Rock Failure, from P. Van Rensburgen, R.R. Hillis, A.J. Maltman, and C.K. Morley (eds), Subsurface Sediment Mobilization, Geological Society, London, v. 216, pp. 358-368.

Hobbs, P.R.N, J.R. Hallam, A. Forster, D.C. Entwisle, L.D. Jones, A.C. Cripps, K.J. Northmore, S.J. Self, and J.L. Meakin, 2002. Engineering Geology of British Rocks and Soils - Mudstones of the Mercia Mudstone Group, British Geological Survey Urban Geoscience and Geological Hazards Programme Research Report RR/01/02.

Horseman, S.T. and J.F. Harrington, 1996. Evidence for Thresholds, Pathways, and Intermittent Flow in Argillaceous Rocks, from Fluid Flow through Faults and Fractures in Argillaceous Formations, A Joint NEA/EC Workshop, Berne, Switzerland, June 10-12, 1996.

Horseman, S.T., J.J.W. Higgo, J. Alexander, and J.F. Harrington, 1996. Water, Gas and Solute Movement Through Argillaceous Media, for the NEA Working Group on Measurement and Physical Understanding of Groundwater Flow Through Argillaceous Media ("Clay Club") a Sub-group of the NEA Co-ordinating Group on Site Evaluation and Design of Experiments for Radioactive Waste Disposal (SEDE) REPORT CC-96/1.

Houseworth, J., and P. Persoff, 2012. Disposal System Material Properties for Near-Field Modeling of a Clay Repository, DOE-NE Used Fuel Disposition Campaign Report. Lawrence Berkeley National Laboratory.

Ingram, G.M. and J.L. Urai, 1999. Top-seal Leakage Through Faults and Fractures: The Role of Mudrock Properties, from A.C. Aplin, A.J. Fleet, J.H.S. Macquaker (eds) Muds and Mudstones: Physical and Fluid Flow Properties. Geological Society, London, Special Publications, v. 158, pp. 125-135.

Ishii, E., H. Funaki, T. Tokiwa, K. Ota, 2010. Relationship Between Fault Growth Mechanism and Permeability Variations With Depth of Siliceous Mudstones in Northern Hokkaido, Japan, Journal of Structural Geology, v. 32, pp. 1792–1805.

Ishii, E., H. Sanada, H. Funaki, Y. Sugita, and H. Kurikami, 2011. The Relationships among Brittleness, Deformation Behavior, and Transport Properties in Mudstones: An Example from the Horonobe Underground Research Laboratory, Japan, Journal of Geophysical Research, v. 116, 15 pp.

Keskin, S.N., M.A. Tekinsoy, S. Uzundurukan, 2004. The Effects of Over Consolidation Ratio and Effective Stresses to the Earth Pressure at Rest at Clay Soils, Teknik Dergi, v. 15, no. 3, pp: 3295-3310.

Lahann R.W. and R. E. Swarbrick, 2011. Overpressure Generation by Load Transfer Following Shale Framework Weakening due to Smectite Diagenesis, Geofluids, v. 11, pp. 362–375.

Liu, H.H., J. Houseworth, J. Rutqvist, L. Li, D. Asahina, F. Chen, and J. Birkholzer, 2012. Report on Modeling Coupled Processes in the Near Field of a Clay Repository, DOE-NE Used Fuel Disposition Campaign Report. Lawrence Berkeley National Laboratory.

Loucks, R.G., R.M. Reed, S.C. Ruppel, and U. Hammes, 2012. Spectrum of Pore Types and Networks in Mudrocks and a Descriptive Classification for Matrix-Related Mudrock Pores, AAPG Bulletin, v. 96, no. 6, pp. 1071–1098.

Maltman, A. 1994. The Geological Deformation of Sediments. Chapman mad Hall, London.

Manga, M., and C.Y. Wang, 2007. Earthquake Hydrology, In: H. Kanamori (ed.) Treatise on Geophysics, 4, Elsevier, Ch. In: Treatise on Geophysics, G. Schubert (ed.), Vol 4., 293-320.

Manzocchi,T., J.J. Walsh, P. Nell, and G. Yielding, 1999. Fault Transmissibility Multipliers for Flow Simulation Models, Petroleum Geoscience, v. 5, pp. 53– 63.

Martinsen, R.S., 1994. Summary of Published Literature on Anomalous Pressures: Implications for the Study of Pressure Compartments, Chapter 2 from AAPG Memoir 61: Basin Compartments and Seals, Edited by Peter J. Ortoleva.

Mazurek, M., P. Alt-Epping, A. Bath, T. Gimmi, H.N. Waber, S. Buschaert, P. De Cannière, M. De Craen, A. Gautschi, S. Savoye, A. Vinsot, I. Wemaere, L. Wouters, 2011. Natural Tracer Profiles across Argillaceous Formations, Applied Geochemistry, v. 26, pp. 1035–1064.

Mertens, J., N. Vandenberghe, L. Wouters, M. Sintubin, 2003. The Origin and Development of Joints in the Boom Clay Formation (Rupelian) in Belgium, from P. Van Rensburgen, R.R. Hillis, A.J. Maltman, and C.K. Morley (eds), Subsurface Sediment Mobilization, Geological Society, London, v. 216, pp. 358-368.

Neuzil, C.E., 1986. Groundwater Flow in Low-Permeability Environments, Water Resources Research, v. 22, no. 8, pp. 1163-1195.

Neuzil, C.E., 1994. How Permeable are Clays and Shales?, Water Resources Research, v. 30, no. 2, pp. 145-15.

Neuzil, C.E., 1995. Abnormal Pressures as Hydrodynamic Phenomena, American Journal of Science, v. 295, pp. 742-786.

Neuzil, C.E., 2000. Osmotic Generation of 'Anomalous' Fluid Pressures in Geological Environments, Nature v. 403, pp. 182-184.

Neuzil, C.E., and A.M. Provost, 2009. Recent Experimental Data May Point to a Greater Role for Osmotic Pressures in the Subsurface, Water Resources Research, v. 45, 14 pp.

Nygård, R., M. Gutierrez, R.K. Bratli, and K. Høeg, 2006. Brittle–Ductile Transition, Shear Failure and Leakage in Shales and Mudrocks, Marine and Petroleum Geology, v. 23, pp. 201–212.

Oldenburg, C.M. and K. Pruess, 1995. EOS7R: Radionuclide Transport for TOUGH2, Lawrence Berkeley National Laboratory Report LBL-34868.

Olson, J.E., 2004. Predicting Fracture Swarms - The Influence of Subcritical Crack Growth and the Crack-Tip Process Zone on Joint Spacing in Rock, from J.W. Cosgrove, and T. Engelder (eds), The Initiation, Propagation, and Arrest of Joints and Other Fractures. Geological Society, London, Special Publications, v. 231, pp. 73-87.

Osborne, M.J. and R.E. Swarbrick, 1997. Mechanisms for Generating Overpressure in Sedimentary Basins: A Reevaluation, AAPG Bulletin, v. 81, no. 6, pp. 1023–1041.

Potter, P.E.; Maynard, J.B.; Depetris, P.J. 2005. "Mud and Mudstones Introduction and Overview; Chapter 6. Burial", Springer-Verlag Berlin Heidelberg, pp. 127-155.

Richardson, R.M. and S.C. Solomon, 1977. Apparent Stress and Stress Drop for Intraplate Earthquakes and Tectonic Stress in the Plates, Pageoph, v. 115, pp. 317-331.

Sales, J.K., 1997. Seal Strength vs. Trap Closure — A Fundamental Control on the Distribution of Oil and Gas, in R.C. Surdam, ed., Seals, traps, and the petroleum system: AAPG Memoir v. 67, pp. 57–83.

Schmatz, J., P.J. Vrolijk, J.L. Urai, 2010. Clay Smear in Normal Fault Zones – The Effect of Multilayers and Clay Cementation in Water-Saturated Model Experiments, Journal of Structural Geology, v. 32, pp. 1834–1849.

Shohet, D.C., 2008. Estimation of Mean Effective Stress in Clay Soils, Geotechnical Engineering, v. 161, Issue GE3.

Sibson, R.H., 1990. Conditions for Fault-Valve Behavior, from R.J. Knipe and E.H. Rutter (eds), Deformation Mechanisms, Rheology and Tectonics, Geological Society Special Publication No. 54, pp. 15-28.

Strout, J.M. and T.I. Tjelta, 2005. In Situ Pore Pressures: What is their significance and how can they be reliably measured?, Marine and Petroleum Geology, v. 22, pp. 275–285.

Stump, B.B., P.B. Flemings, T. Finkbeiner, M.D. Zoback, 1999. Pressure Differences Between Overpressured Sands and Bounding Shales of the Eugene Island 330 field (Offshore Louisiana, U.S.A.) with Implications for Fluid Flow, Mitchell, A., Grauls, D. (eds). 1999 Overpressure in Petroleum Exploration - Proc. Workshop Pau, April 7-8, 1998; Bull. Centre Rech. Elf Explor. Prod. Mem. 22, 248 pp. 215.

Swarbrick, R.E. and M.J. Osborne, 1998, Mechanisms that Generate Abnormal Pressures: An Overview, in B.E. Law, G.F. Ulmishek, and V.I. Slavin eds., Abnormal pressures in hydrocarbon environments: AAPG Memoir 70, p. 13–34.

Swarbrick, R.E., 2002. Challenges of Porosity-Based Pore Pressure Prediction, CSEG Recorder.

Terzaghi, K. and F. E. Richart, Jr. 1952. Stresses in rock about cavities. Geotechnique. Vol. 2, No. 3, pp. 57–90.

Tingay, M.R.P., R.R. Hillis, C.K. Morley, R.E. Swarbrick, and E.C. Okpere, 2003. Pore Pressure/Stress Coupling in Brunei Darussalam - Implications for Shale Injection, from P. Van Rensburgen, R.R. Hillis, A.J. Maltman, and C.K. Morley (eds), Subsurface Sediment Mobilization, Geological Society, London, v. 216, pp. 358-368.

USGS http://tin.er.usgs.gov/geology/state/sgmc-lith.php?text=mudstone

Warpinski, N.R., J. Du, and U. Zimmer, 2012. Measurements of Hydraulic-Fracture-Induced Seismicity in Gas Shales, SPE 151957, SPE Hydraulic Fracturing Technology Conference, The Woodlands, Texas, USA, February 6-8.

Wesley, L.D., 2010. Fundamentals of Soil Mechanics for Sedimentary and Residual Soils, John Wiley and Sons, Inc.

White, W.A., 1949. Atterberg Plastic Limits of Clay Minerals, American Mineralogist, v. 34, pp. 508-512.

Wolf, L.W., M.-K. Lee, S. Browning, and M.P. Tuttle, 2009. Numerical Analysis of Overpressure Development in the New Madrid Seismic Zone, Bulletin of the Seismological Society of America, v. 95, no. 1, pp. 135–144.

Wong T.-F. and W. Zhu, 1999. Brittle Faulting and Permeability Evolution: Hydromechanical Measurement, Microstructural Observation, and Network Modeling, from W.C. Haneberg, P.S. Mozley, J.C. Moore, and L.B. Goodwin (eds), Faults and Subsurface Fluid Flow in the Shallow Crust, American Geophysical Union.

Yielding, G., B. Freeman, and D.T. Needham, 1997. Quantitative Fault Seal Prediction, AAPG Bulletin, v. 81, no. 6, pp. 897–917.

Zanbak, C. and R.C. Arthur, 1984. Rock Mechanics Aspects of Volume Changes In Calcium Sulfate Bearing Rocks Due To Geochemical Phase Transitions, 25th U.S. Symposium on Rock Mechanics (USRMS), June 25 - 27, 1984, Evanston, IL.